A Nonlinear Least Squares Method for Solving the Joint Reconstruction and Registration Problem in Digital Breast Tomosynthesis[†]

Guang Yang, John H. Hipwell
{g.yang,j.hipwell}@cs.ucl.ac.uk
David J. Hawkes, Simon R. Arridge
{d.hawkes,simon.arridge}@cs.ucl.ac.uk

Centre for Medical Image Computing
Department of Computer Science
and Medical Physics
University College London
London, UK, WC1E 6BT

Abstract

Digital Breast Tomosynthesis (DBT) offers potential insight into the fine details of normal fibroglandular tissues and abnormal lesions, e.g., masses and micro-calcifications associated with breast cancer, by the production of a pseudo-3D image. In addition, it avoids the superposition, which is usually found in X-ray mammography, with a comparable radiation dose. Algorithms to aid the human observer process DBT data sets involve two key tasks: reconstruction and registration. In established medical image modalities these tasks are normally performed sequentially; the images are reconstructed and then registered. In this paper, we hypothesise that, for DBT in particular, combining the optimisation processes of reconstruction and registration into a single algorithm will offer satisfactory for both tasks. Based on this hypothesis, we have devised a mathematical framework to combine these two tasks, and have implemented both affine and non-linear B-spline registration transformation models as plug-ins. By applying our algorithm to various simulated data, we demonstrate the success of our method in terms of both reconstruction fidelity and in the registration accuracy of the recovered transformations.

1 Introduction

Digital breast tomosynthesis (DBT), is a tomographic modality in which a volumetric image is reconstructed from the acquisition of multiple X-ray images over a limited angular range [3]. By acquiring a 3D image, albeit with coarse depth resolution, DBT aims to disambiguate the overlapping tissues that degrade the sensitivity and the specificity of conventional mammography. In so doing, DBT could be a suitable complementary imaging modality to mammography, enhancing the performance of screening and diagnosis of breast cancer by clinicians.

The workflow in which DBT would be used clinically, involves two key tasks: reconstruction, to generate a 3D image of the breast, and registration, to enable images from different visits to be compared, a task that is routinely performed by radiologists working

[†]Contact Email: G.Yang@cs.ucl.ac.uk. This work has been funded by DTI Project *Digital Breast Tomosynthesis* TP/7/SEN/6/1/M1577G. The authors would like to thank the UK MR Breast Screening Study (MARIBS) for providing the data for this study.

with conventional mammograms. In other modalities, such as MRI and CT, these tasks have traditionally been performed sequentially, i.e. the temporal data sets are first reconstructed independently and then registered. This can be effective if reconstructing using a complete set of data. However, for ill-posed limited-angle problems such as DBT, estimating the deformation is challenging due to the presence of significant reconstruction artefacts, which can lead to severe inaccuracies in the registration.

In this paper, we hypothesise that combining the reconstruction and registration of DBT into a single process will offer satisfactory for both tasks. There is little previous research in this field, and existing techniques applied to modalities other than DBT have focussed on either 2D affine or 3D rigid motion correction rather than 3D affine and non-rigid B-spline implemented in our method. Chung et al. [1] elucidated a combined framework to solve the super-resolution problem of motion correction in MR images, using a 2D affine model. In 2009, Schumacher et al. [2] proposed a method to combine reconstruction and motion correction for SPECT imaging, but only considered 3D rigid motion. The authors have approached the combined problem in DBT using an iterative method before [4, 5].

In addition to the novelty of our fully-coupled simultaneous approach (cf. the iterative method) in incorporating more complex transformation models, we also address the challenging task of applying these techniques to the limited angle datasets acquired in DBT. We test and validate this method using various phantom data, breast MRI, and simulated breast images.

2 Method

Forward Problem: A 3D image, $\mathrm{f}_1^{\mathrm{g}} \in \mathbb{R}^{\mathrm{D}_3}$, two sets of temporal data, p_1, $\mathrm{p}_2 \in \mathbb{R}^{p_{\mathrm{num}} \times \mathrm{D}_2}$, the parametric transformations, $\mathscr{T}_\zeta^{\mathrm{g}}$, and the system matrix, $A \in \mathbb{R}^{p_{\mathrm{num}} \times \mathrm{D}_2 \times \mathrm{D}_3} : \mathbb{R}^{\mathrm{D}_3} \mapsto \mathbb{R}^{\mathrm{D}_2}$, can be related via

$$\mathrm{p}_1 = A\mathrm{f}^{\mathrm{g}} = A\mathrm{R}(\mathrm{x}); \tag{1}$$

$$\mathrm{p}_2 = A\mathscr{T}_\zeta^{\mathrm{g}}\mathrm{f}^{\mathrm{g}} = A\mathrm{T}[\mathscr{T}_\zeta(\mathrm{x})], \tag{2}$$

where p_{num} is the number of limited angle projections, and D_2 and D_3 denote the 3D volume space and 2D projection space. In addition, $\mathrm{f}_1^{\mathrm{g}}$ and $\mathscr{T}_\zeta^{\mathrm{g}}$ are the ground truth of the reconstruction and the parametric transformations respectively, whilst R and T represent the interpolations at original coordinates x and transformed coordinates $\mathscr{T}_\zeta(\mathrm{x})$.

Inverse Problem: We solve the inverse problem by forming the objective function given by

$$\{\mathrm{f}^\star, \zeta^\star\} = \arg\min_{\mathrm{f},\zeta} \left(f(\mathrm{f},\zeta) = \frac{1}{2}\left(\left\|A\mathrm{f} - \mathrm{p}_1\right\|^2 + \left\|A\mathscr{T}_\zeta\mathrm{f} - \mathrm{p}_2\right\|^2\right)\right), \tag{3}$$

in which f denotes the estimation of the unknown volume, and ζ is the estimation of the unknown parametric transformations.

A minimiser $\{\mathrm{f}^\star, \zeta^\star\} \in \mathbb{R}^n$ of $f(\mathrm{f},\zeta)$ is characterised by the necessary condition that the partial derivative with respect to f and ζ equals zero. The partial derivative with respect to f is straightforward, and is given by

$$g(\mathrm{f}) = \frac{\partial f(\mathrm{f},\zeta)}{\partial \mathrm{f}} = A^T(A\mathrm{f} - \mathrm{p}_1) + \mathscr{T}_\zeta^* A^T(A\mathscr{T}_\zeta\mathrm{f} - \mathrm{p}_2), \tag{4}$$

in which $g(\mathrm{f})$ is the gradient with respect to f, and $\mathscr{T}_\zeta^*$ is the adjoint operator of $\mathscr{T}_\zeta$.

To derive the partial derivative with respect to ζ, we apply a small perturbation to the objective function and the linearisation via the norm yields,

$$f\left(\mathrm{f},\zeta+\Delta\zeta\right)=\frac{1}{2}\left(\left\|A\mathrm{f}-\mathrm{p}_1\right\|^2+\left\|A\mathscr{T}_{\zeta+\Delta\zeta}\mathrm{f}-\mathrm{p}_2\right\|^2\right) \tag{5}$$

$$\approx\frac{1}{2}\left(\left\|A\mathrm{f}-\mathrm{p}_1\right\|^2+\left\|A\mathscr{T}_{\zeta}\mathrm{f}+A\frac{\partial\mathscr{T}_{\zeta}}{\partial\zeta}\mathrm{f}\Delta\zeta-\mathrm{p}_2\right\|^2\right). \tag{6}$$

If $g(\zeta)$ denotes the gradient then we have,

$$g(\zeta)=\frac{\partial f(\mathrm{f},\zeta)}{\partial\zeta}=\left(A\frac{\partial\mathscr{T}_{\zeta}}{\partial\zeta}\mathrm{f}\right)^T\left(A\mathscr{T}_{\zeta}\mathrm{f}-\mathrm{p}_2\right)=\left(A\mathscr{T}'_{\zeta}\mathrm{f}\right)^T\left(A\mathscr{T}_{\zeta}\mathrm{f}-\mathrm{p}_2\right).$$

Adjoint Operator of the Transformations: The adjoint operator of the transformation, denoted by $\mathscr{T}^*$, is used to solve the inverse problem. The definition of the adjoint operator in the context of linear transformations on finite dimensional vector spaces is straightforward. By adopting a matrix representation of the linear transformations, we utilise the fact that the adjoint of such a matrix is the same as its transpose.

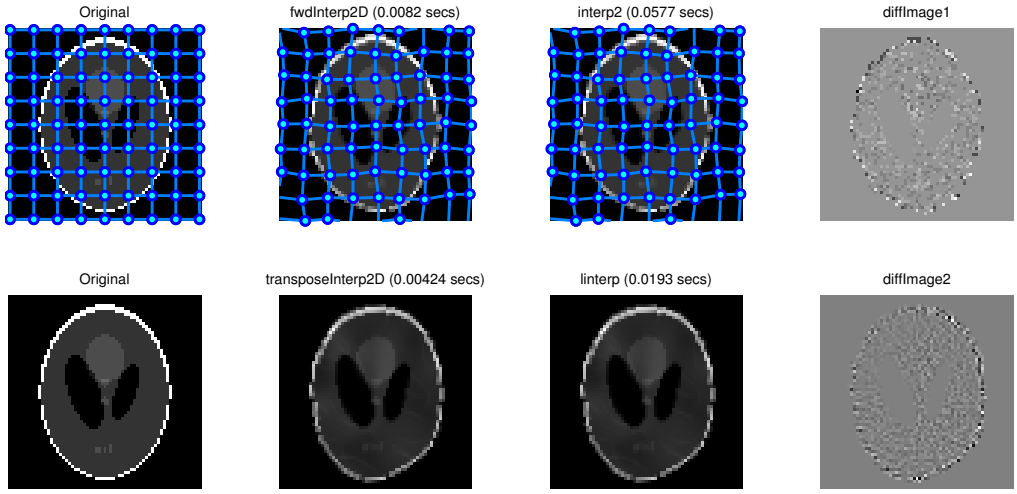

Figure 1: *2D results of the interpolation operation and its transpose. First row: Forward interpolation with deformed grid on; Second row: transpose of the interpolation. From left to right: Original image; Implementation using C with Matlab MEX interfaces; Implementation using Matlab; Difference images between two implementations. The results have shown that our C implementation is faster and accurate.*

The adjoint operator, also known as the Hermitian conjugate, can be defined by

$$\left\langle\mathscr{T}(\mathrm{f}_1),\mathrm{f}_2\right\rangle=\left\langle\mathrm{f}_1,\mathscr{T}^*(\mathrm{f}_2)\right\rangle \tag{7}$$

in which $\langle\cdot,\cdot\rangle$ is the inner product. f_1 and f_2 are arbitrary vectors such that $\forall\mathrm{f}_1,\mathrm{f}_2\in\mathrm{H}_s$, where H_s denotes the Hilbert space; a vector space with an inner product with respect to the associated norm. Although $\mathscr{T}$ is nonlinear with respect to the transformation, ζ, it is linear with respect to the image intensities f. Since $\mathscr{T}_{\zeta}\mathrm{f}=\mathrm{T}[\mathscr{T}_{\zeta}(\mathrm{x})]$,

$$\mathscr{T}_{\zeta}^*\mathrm{f}=\mathscr{T}_{\zeta}^T\mathrm{f}=\mathrm{T}^T[\mathscr{T}_{\zeta}(\mathrm{x})]. \tag{8}$$

In other words, the transpose of an image transformation is the transpose of an interpolation operation. To illustrate this property we implemented both the image interpolation (bilinear interpolation) and the equivalent transpose operation and applied them to 2D (Fig. 1)

and 3D (Fig. 2) test images using randomly created B-spline transformations. In addition, we validated our implementation using Equation 7 with an arbitrary image, to test various transformations. In all cases we obtained the same inner product results.

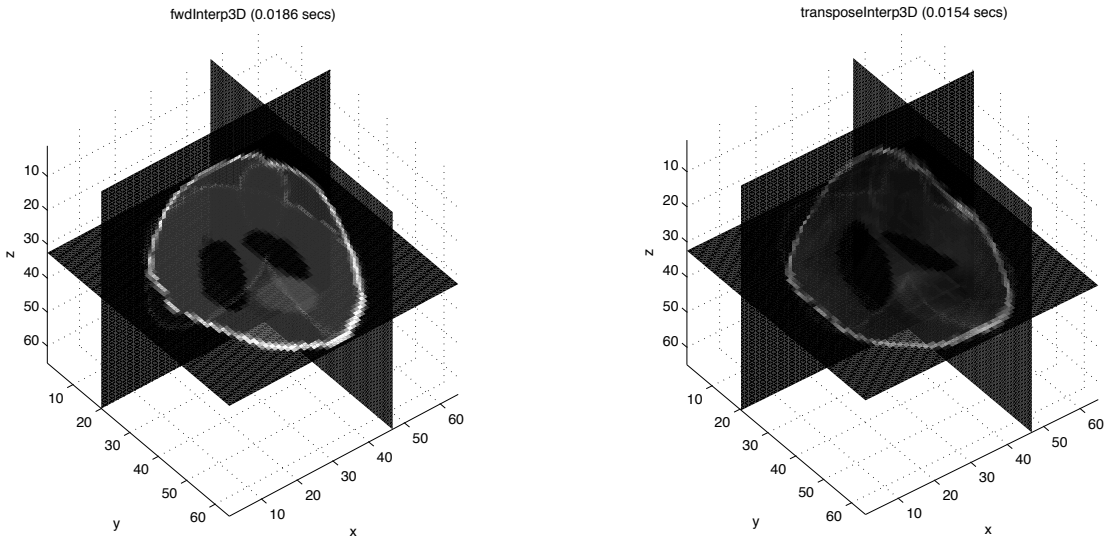

Figure 2: *3D results of the interpolation operation (Left) and its transpose (Right).*

Derivative Operator of the Transformations: The derivative of the transformation operation is a key component of the algorithm and has great impact on the result of the optimisation. Deriving an analytical derivative of the transformation is desirable because it would be fast to compute but is complicated by the need to formulate the derivative of the underlying interpolation. In addition, some interpolation schemes have no analytical derivative. For this reason therefore, we use the Finite Difference Method (FDM) to approximate the derivative operation:

$$\mathscr{T}_{\zeta}^{'} \approx \frac{\mathscr{T}_{\zeta+\varepsilon} + \mathscr{T}_{\zeta-\varepsilon}}{2\varepsilon} \tag{9}$$

where ε is a small number.

Optimisation: The optimisation is performed using a quasi-Newton based Limited Memory BFGS (L-BFGS) method. This approximates the inverse of the Hessian matrix whilst avoiding the considerable memory overhead (for large DBT data sets) associated with computing 2nd order derivatives or their fully dense approximations directly.

3 Results

In this section we investigate the performance of our framework using (a) an affine transformation model and (b) a non-rigid B-spline transformation model.

Affine based experiments: In the first experiment, a 3D toroidal phantom image was created, and subjected to 20 affine transformations to test the robustness of our joint method. In the second experiment, 15 randomly generated affine transformations were applied to a 3D breast MR image. The specific parameters recovered are shown in Fig. 3. In a third experiment, we tested the methods using two MRI acquisitions obtained before and after application of a lateral-to-medial plate compression of the breast. There is no ground truth for the deformation of this dataset, however from the mean squared error (MSE in Table 1), we can conclude that our joint method has successfully reconstructed the data with reasonable registration.

B-spline based experiments: In the fourth experiment, we created a 3D Shepp-Logan phantom image. Although the 3D Shepp-Logan phantom does not represent the structure of the breast, it is a widely used phantom image for tomographic reconstruction. Fig. 4(a) shows central orthogonal slices through the 3D Shepp-Logan phantom ($65 \times 65 \times 65$ in voxels), and the regular grid of B-spline control points for the central slice of the transverse plane. The transformed phantom is shown in Fig. 4(b), with the ground truth transformation. This ground truth deformation is randomly simulated with 9 control points in each dimension using the B-spline transformation model. From the results shown in Figs. 4(c) and (d), we can conclude that our joint method has obtained a reconstruction in high fidelity with an accurate recovery of the non-rigid deformation.

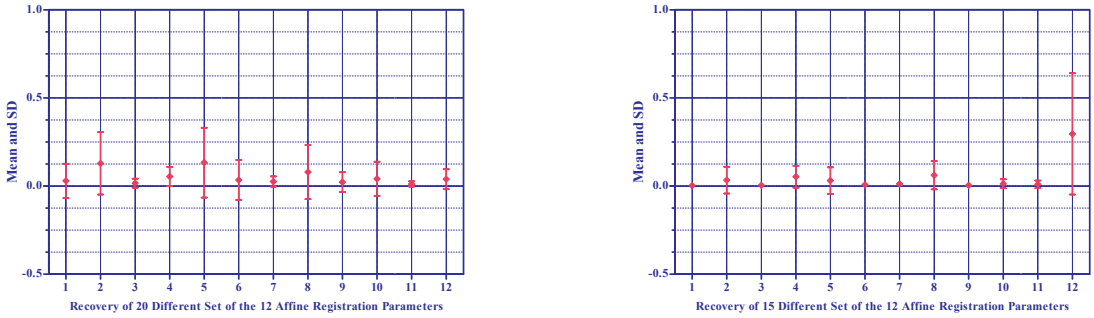

Figure 3: *Mean and standard deviation of the absolute error between the recovered and the ground truth of different sets of affine transformations. Parameters 4, 8, and 12 are the translations along each axis. (Left: Experiment on a 3D toroidal phantom image with 20 randomly created affine transformations; Right: Experiment on a 3D breast MRI image with 15 randomly created affine transformations. The translation could be measured in voxels; however, other parameters have no defined unit because they are calculated using matrices multiplication, e.g., 3D rotation matrix is multiplied by 3D shearing matrix and etc.)*

Table 1: *Comparison of the MSE error* $\frac{1}{\mathbb{N}}\|\mathrm{f}^{\star} - \mathrm{f}^{\mathrm{g}}\|^2$ *before and after performing our joint reconstruction and registration* ($\mathbb{N}$ *is the number of voxels*).

	Initial	**Joint Method**
Toroid Phantom	5.66×10^6	0.24×10^3
Uncompressed Breast MRI	1.18×10^6	3.01×10^3
In vivo DBT simulation	5.32×10^6	3.22×10^4

4 Conclusion

We have presented a method to jointly reconstruct and register temporal DBT datasets and tested it using both affine and B-spline transformation models. Our work has led us to conclude that this joint method produced satisfactory results in both registration accuracy and reconstruction appearance. Furthermore, our framework should be straightforward to incorporate other non-rigid transformation models and priors to regularise the solution. This method has application for the detection of change in temporal DBT data sets. It may also be applied to the combined reconstruction and registration of two view (cranial-caudal (CC) and Mediolateral-oblique (MLO)) DBT data sets, to overcome the null-space limitation of the individual views and produce a single reconstructed volume with improved depth resolution.

References

[1] Chung, J., et al.: Numerical methods for coupled superresolution. Inverse Problems, Vol. 22(4), pp. 1261 (2006)

[2] Schumacher, H., et al.: Combined reconstruction and motion correction in SPECT imaging. Nuclear Science, IEEE Transactions on, Vol. 56(9), pp. 73-80 (2009)

[3] Wu, Tao, et al.: A comparison of reconstruction algorithms for breast tomosynthesis. Medical Physics, Vol. 31(9), pp. 2636-2647 (2004)

[4] Yang, Guang, et al.: Combined reconstruction and registration of digital breast tomosynthesis. IWDM'10, LNCS, Vol. 6136, pp. 760-768 (2010)

[5] Yang, Guang, et al.: Combined reconstruction and registration of digital breast tomosynthesis: Sequential method versus iterative method. MIUA'10, pp. 1-5 (2010)

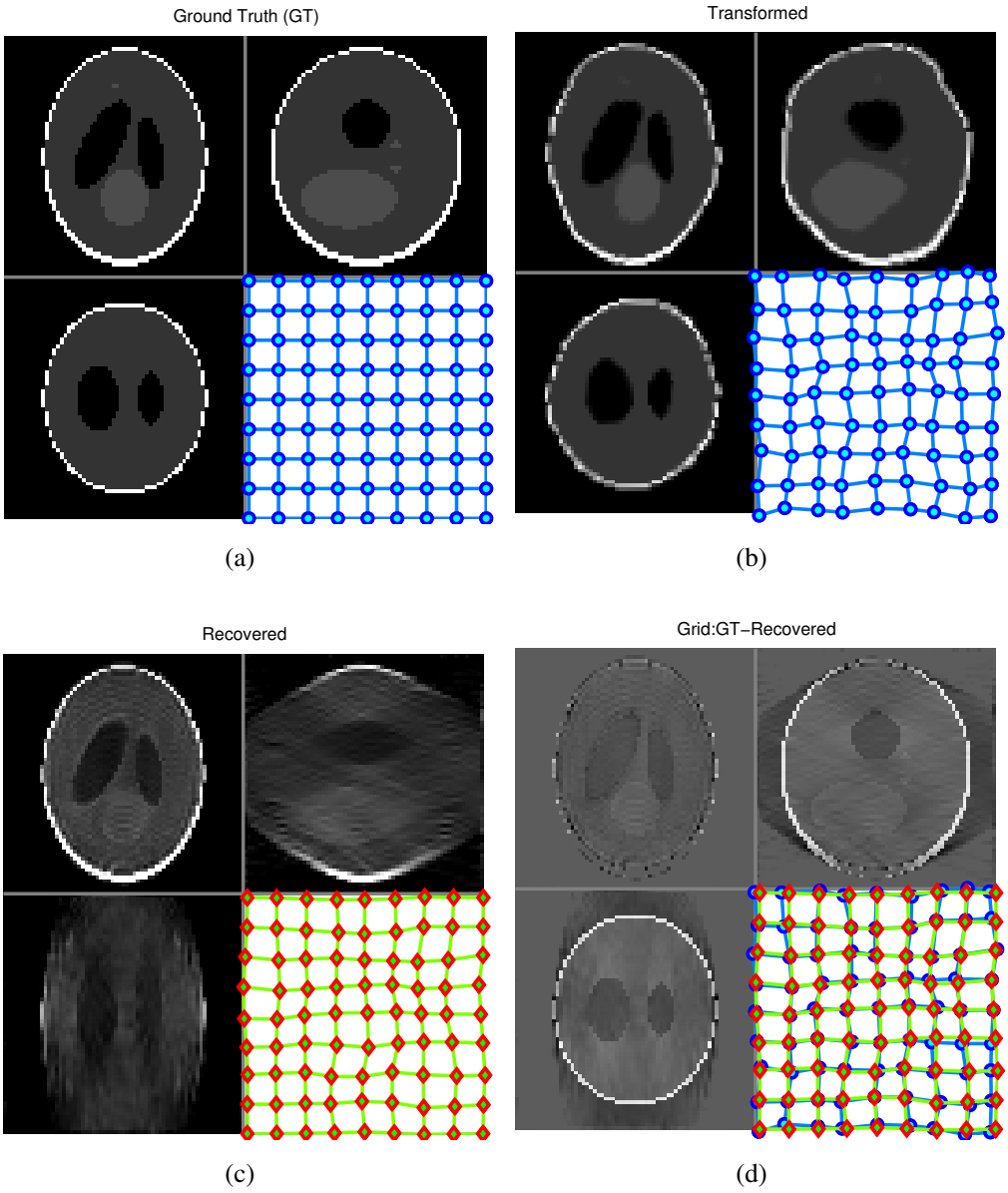

Figure 4: *(a): Original fixed 3D Shepp-Logan phantom and the regular B-spline control point grid for the central slice; (b): Transformed 3D Shepp-Logan phantom and its deformed grid for the central slice, i.e., the ground truth transformation; (c): Joint reconstruction and registration result and its recovered transformation grid for the central slice; (d): Difference image between the joint result and the original fixed image, and the recovered grid superimposed on the ground truth transformation. (Four sub-figures from top to bottom and from left to right are: Transverse view; Coronal view; Sagittal view; Grid of the central slice of the transverse view.)*